We are IntechOpen, the world's leading publisher of Open Access books
Built by scientists, for scientists

6,900
Open access books available

186,000
International authors and editors

200M
Downloads

154
Countries delivered to

Our authors are among the

TOP 1%
most cited scientists

12.2%
Contributors from top 500 universities

CLARIVATE ANALYTICS
BOOK CITATION INDEX
INDEXED

WEB OF SCIENCE™

Selection of our books indexed in the Book Citation Index
in Web of Science™ Core Collection (BKCI)

Interested in publishing with us?
Contact book.department@intechopen.com

Numbers displayed above are based on latest data collected.
For more information visit www.intechopen.com

Transition Modelling for Turbomachinery Flows

F. R. Menter[1] and R. B. Langtry[2]
[1]ANSYS GmbH
[2]The Boeing Company,
[1]Germany
[2]USA

1. Introduction

In the past few decades a significant amount of progress has been made in the development of reliable turbulence models that can accurately simulate a wide range of fully turbulent engineering flows. The efforts by different groups have resulted in a spectrum of models that can be used in many different applications, while balancing the accuracy requirements and the computational resources available to a CFD user. However, the important effect of laminar-turbulent transition is not included in the majority of today's engineering CFD simulations. The reason for this is that transition modelling does not offer the same wide spectrum of CFD-compatible model formulations that is currently available for turbulent flows, even though a large body of publications is available on the subject. There are several reasons for this unsatisfactory situation.

The first is that transition occurs through different mechanisms in different applications. In aerodynamic flows, transition is typically the result of a flow instability (Tollmien-Schlichting waves or in the case of highly swept wings cross-flow instability), where the resulting exponential growth of two-dimensional waves eventually results in a non-linear break-down to turbulence. Transition occurring due to Tollmien-Schlichting waves is often referred to as natural transition [1]. In turbomachinery applications, the main transition mechanism is bypass transition [2] imposed on the boundary layer by high levels of turbulence in the freestream. The high freestream turbulence levels are for instance generated by upstream blade rows. Another important transition mechanism is separation-induced transition [3], where a laminar boundary layer separates under the influence of a pressure gradient and transition develops within the separated shear layer (which may or may not reattach). As well, a turbulent boundary layer can re-laminarize under the influence of a strong favorable pressure gradient [4]. While the importance of transition phenomena for aerodynamic and heat transfer simulations is widely accepted, it is difficult to include all of these effects in a single model.

The second complication arises from the fact that conventional Reynolds averaged Navier-Stokes (RANS) procedures do not lend themselves easily to the description of transitional flows, where both linear and non-linear effects are relevant. RANS averaging eliminates the

effects of linear disturbance growth and is therefore difficult to apply to the transition process. While methods based on the stability equations such as the e^n method of Smith & Gamberoni [5] and van Ingen [6] avoids this limitation, they are not compatible with general-purpose CFD methods as typically applied in complex geometries. The reason is that these methods require a priori knowledge of the geometry and the grid topology. In addition, they involve numerous non-local operations (e.g. tracking the disturbance growth along each streamline) that are difficult to implement into today's CFD methods [7]. This is not to argue against the stability approaches, as they are an essential part of the desired "spectrum" of transition models required for the vastly different application areas and accuracy requirements. However, much like in turbulence modeling, it is important to develop engineering models that can be applied in day-to-day operations by design engineers on complicated 3D geometries.

It should be noted that at least for 2D flows, the efforts of various groups has resulted in a number of engineering design tools intended to model transition for very specific applications. The most notable efforts are those of Drela and Giles [8] who developed the XFOIL code which can be used for modeling transition on 2D airfoils and the MISES code of Youngren and Drela [9], which is used for modeling transition on 2D turbomachinery blade rows. Both of these codes use a viscous – inviscid coupling approach which allows the classical boundary layer formulation tools to be used. Transition prediction is accomplished using either an e^n method or an empirical correlation and both of these codes are used widely in their respective design communities. A 3D wing or blade design is performed by stacking the 2D profiles (with the basic assumption that span wise flow is negligible) to create the geometry at which point a 3D CFD analysis is preformed.

Closer inspection shows that hardly any of the current transition models are CFD-compatible. Most formulations suffer from non-local operations that cannot be carried out (with reasonable effort) in general-purpose CFD codes. This is because modern CFD codes use mixed elements and massive parallel execution and do not provide the infrastructure for computing integral boundary layer parameters or allow the integration of quantities along the direction of external streamlines. Even if structured boundary layer grids are used (typically hexahedra), the codes are based on data structures for unstructured meshes. The information on a body-normal grid direction is therefore not easily available. In addition, most industrial CFD simulations are carried out on parallel computers using a domain decomposition methodology. This means in the most general case that boundary layers can be split and computed on different processors, prohibiting any search or integration algorithms. Consequently, the main requirements for a fully CFD-compatible transition model are:

- Allow the *calibrated* prediction of the onset and the length of transition
- Allow the inclusion of different transition mechanisms
- Be formulated locally (no search or line-integration operations)
- Avoid multiple solutions (same solution for initially laminar or turbulent boundary layer)
- Do not affect the underlying turbulence model in fully turbulent regimes
- Allow a robust integration down to the wall with similar convergence as the underlying turbulence model
- Be formulated independent of the coordinate system
- Applicable to three-dimensional boundary layers

Considering the main classes of engineering transition models (stability analysis, correlation based models, low-Re models) one finds that none of these methods can meet all of the above requirements.

The only transition models that have historically been compatible with modern CFD methods are the low-Re models [10,11]. However, they typically suffer from a close interaction with the transition capability and the viscous sublayer modeling and this can prevent an independent calibration of both phenomena [12, 13]. At best, the low-Re models can only be expected to simulate bypass transition which is dominated by diffusion effects from the freestream. This is because the standard low-Re models rely exclusively on the ability of the wall damping terms to capture the effects of transition. Realistically, it would be very surprising if these models that were calibrated for viscous sublayer damping could faithfully reproduce the physics of transitional flows. It should be noted that there are several low-Re models where transition prediction was considered specifically during the model calibration [14, 15, 16]. However, these model formulations still exhibit a close connection between the sublayer behavior and the transition calibration. Re-calibration of one functionality also changes the performance of the other. It is therefore not possible to introduce additional experimental information without a substantial re-formulation of the entire model.

The engineering alternative to low-Re transition models are empirical correlations such as those of [17, 18 and 19]. They typically correlate the transition momentum thickness Reynolds number to local freestream conditions such as the turbulence intensity and pressure gradient. These models are relatively easy to calibrate and are often sufficiently accurate to capture the major effects of transition. In addition, correlations can be developed for the different transition mechanisms, ranging from bypass to natural transition as well as crossflow instability or roughness. The main shortcoming of these models lies in their inherently non-local formulation. They typically require information on the integral thickness of the boundary layer and the state of the flow outside the boundary layer. While these models have been used successfully in special-purpose turbomachinery codes, the non-local operations involved with evaluating the boundary layer momentum thickness and determining the freestream conditions have precluded their implementation into general-purpose CFD codes.

Transition simulations based on linear stability analysis such as the e^n method are the lowest closure level available where the actual instability of the flow is simulated. In the simpler models described above, the physics is introduced through the calibration of the model constants. However, even the e^n method is not free from empiricism. This is because the transition n-factor is not universal and depends on the wind tunnel freestream/acoustic environment and also the smoothness of the test model surface. The main obstacle to the use of the e^n model is that the required infrastructure needed to apply the model is very complicated. The stability analysis is typically based on velocity profiles obtained from highly resolved boundary layer codes that must be coupled to the pressure distribution of a RANS CFD code [7]. The output of the boundary layer method is then transferred to a stability method, which then provides information back to the turbulence model in the RANS solver. The complexity of this set-up is mainly justified for special applications where the flow is designed to remain close to the stability limit for drag reduction, such as laminar wing design.

Large Eddy Simulation (LES) and Direct Numerical Simulations (DNS) are suitable tools for transition prediction [20], although the proper specification of the external disturbance level and structure poses substantial challenges. Unfortunately, these methods are far too costly for engineering applications. They are currently used mainly as research tools and substitutes for controlled experiments.

Despite its complexity, transition should not be viewed as outside the range of RANS methods. In many applications, transition is enforced within a narrow area of the flow due to geometric features (e.g. steps or gaps), pressure gradients and/or flow separation. Even relatively simple models can capture these effects with sufficient engineering accuracy. The challenge to a proper engineering model is therefore mainly in the formulation of a model that can be implemented into a general RANS environment.

In this chapter a novel approach to simulating laminar to turbulent transition is described that can be implemented into a general RANS environment. The central idea behind the new approach is that Van Driest and Blumer's [21] vorticity Reynolds number concept can be used to provide a link between the transition onset Reynolds number from an empirical correlation and the local boundary layer quantities. As a result the model avoids the need to integrate the boundary layer velocity profile in order to determine the onset of transition and this idea was first proposed by [22].

Recently another class of locally formulated transition models have been proposed. They are based on modelling the laminar kinetic energy which is present already upstream of the actual transition location. This information is then applied to trigger the actual transition process. Methods of this kind have been proposed e.g. by Walters and Cokljat [23] and Pacciani et al. [24]. While the argumentation behind the derivation of these models is rather different from the γ-Re_Θ model, the mechanisms by which transition is triggered is very similar.

The current chapter is largely based on Langtry and Menter [25]. More recent articles on model validation and development can be found in [26-28].

2. Model formulation

2.1 Basic concept

The current approach is based on combining experimental correlations with locally formulated transport equations. The essential quantity to trigger the transition process is the vorticity or alternatively the strain rate Reynolds number which is used in the present model is defined as follows:

$$\mathrm{Re}_v = \frac{\rho y^2}{\mu}\left|\frac{\partial u}{\partial y}\right| = \frac{\rho y^2}{\mu}S \tag{1}$$

where y is the distance from the nearest wall, S is the shear strain rate, ρ is the density and μ is the dynamic viscosity. The vorticity Reynolds number it is a local property and can be easily computed at each grid point in an unstructured, parallel Navier-Stokes code.

A scaled profile of the vorticity Reynolds number is shown in Figure 1 for a Blasius boundary layer. The scaling is chosen in order to have a maximum of one inside the boundary layer. This is achieved by dividing the Blasius velocity profile by the

corresponding momentum thickness Reynolds number and a constant of 2.193. In other words, the maximum of the profile is proportional to the momentum thickness Reynolds number and can therefore be related to the transition correlations [22] as follows:

$$\mathrm{Re}_\theta = \frac{\max\left(\mathrm{Re}_v\right)}{2.193} \qquad (2)$$

Based on this observation, a general framework can be built, which can serve as a local environment for correlation based transition models.
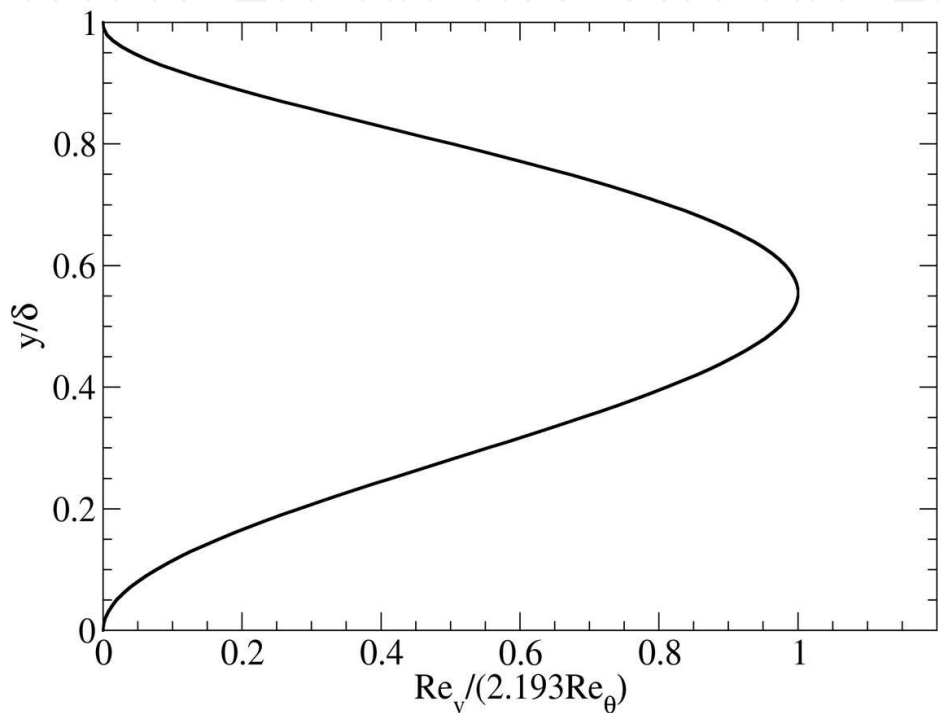

Fig. 1. Scaled vorticity Reynolds number (Re_v) profile in a Blasius boundary layer.

When the laminar boundary layer is subjected to strong pressure gradients, the relationship between momentum thickness and vorticity Reynolds number described by Equation (2) changes due to the change in the shape of the profile. The relative difference between momentum thickness and vorticity Reynolds number, as a function of shape factor (H), is shown in Figure 2. For moderate pressure gradients (2.3 < H < 2.9) the difference between the actual momentum thickness Reynolds number and the maximum of the vorticity Reynolds number is less than 10%. Based on boundary layer analysis a shape factor of 2.3 corresponds to a pressure gradient parameter (λ_θ) of approximately 0.06. Since the majority of experimental data on transition in favorable pressure gradients falls within that range (see for example reference [17]) the relative error between momentum thickness and vorticity Reynolds number is not of great concern under those conditions.

For strong adverse pressure gradients the difference between the momentum thickness and vorticity Reynolds number can become significant, particularly near separation (H = 3.5). However, the trend with experiments is that adverse pressure gradients reduce the transition momentum thickness Reynolds number. In practice, if a constant transition momentum thickness Reynolds number is specified, the transition model is not very
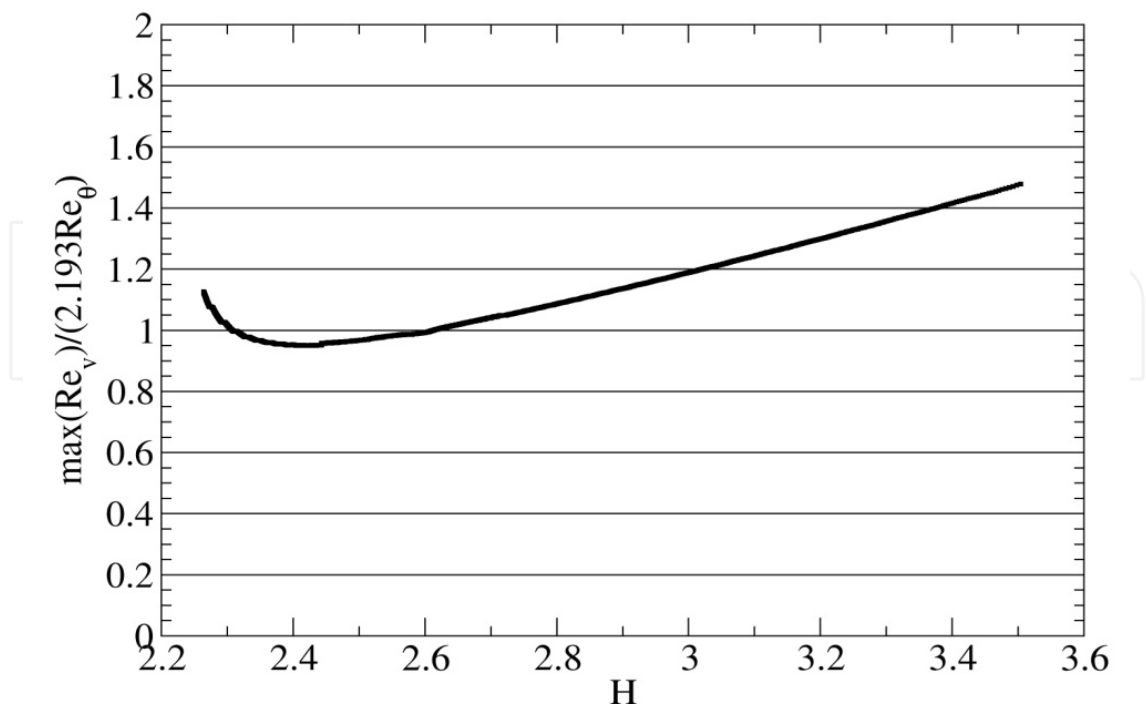
Fig. 2. Relative error between the maximum value of vorticity Reynolds number (Rev) and the momentum thickness Reynolds number (Reθ) as a function of boundary layer shape factor (H).

sensitive to adverse pressure gradients and an empirical correlation such as that of Abu-Ghannam and Shaw [17] is necessary in order to predict adverse pressure gradient transition accurately. In fact, the increase in vorticity Reynolds number with increasing shape factor can actually be used to predict separation induced transition. This is one of the main advantages of the present approach because the standard definition of momentum thickness Reynolds number is not suitable in separated flows.

The function Re_v can be used on physical reasoning, by arguing that the combination of y^2S is responsible for the growth of disturbances inside the boundary layer, whereas $v = \mu / \rho$ is responsible for their damping. As y^2S grows with the thickness of the boundary layer and μ stays constant, transition will take place once a critical value of Re_v is reached. The connection between the growth of disturbances and the function Re_v was shown by Van Driest and Blumer [21] in comparison with experimental data. As well, Langtry and Sjolander [15] found that the location in the boundary layer where Re_v was largest corresponded surprisingly well to the location where the peak growth of disturbances was occurring, at least for bypass transition. The models proposed by Langtry & Sjolander [15] and Walters & Leylek, [16] use Re_v in physics-based arguments based on these observations of disturbance growth in the boundary layer during bypass transition. These models appear superior to conventional low-Re models, as they implicitly contain information of the thickness of the boundary layer. Nevertheless, the close integration of viscous sublayer damping and transition prediction does not easily allow for an independent calibration of both sub-models.

In the present approach first described in references [22, 29, 30 and 31] the main idea is to use a combination of the strain-rate Reynolds number with experimental transition correlations using standard transport equations. Due to the separation of viscous sublayer damping and transition prediction, the new method has provided the flexibility for introducing additional transition effects with relative ease. Currently, the main missing extensions are cross-flow instabilities and high-speed flow correlations and these do not pose any significant obstacles. The concept of linking the transition model with experimental data has proven to be an essential strength of the model and this is difficult to achieve with closures based on a physical modeling of these diverse phenomena.

The present transition model is built on a transport equation for intermittency, which can be used to trigger transition locally. In addition to the transport equation for the intermittency, a second transport equation is solved for the transition onset momentum-thickness Reynolds number. This is required in order to capture the non-local influence of the turbulence intensity, which changes due to the decay of the turbulence kinetic energy in the free-stream, as well as due to changes in the free-stream velocity outside the boundary layer. This second transport equation is an essential part of the model as it ties the empirical correlation to the onset criteria in the intermittency equation. Therefore, it allows the model to be used in general geometries and over multiple airfoils, without additional information on the geometry. The intermittency function is coupled with the SST k-ω based turbulence model [32]. It is used to turn on the production term of the turbulent kinetic energy downstream of the transition point based on the relation between transition momentum-thickness and strain-rate Reynolds number. As the strain-rate Reynolds number is a local property, the present formulation avoids another very severe shortcoming of the correlation-based models, namely their limitation to 2D flows. It therefore allows the simulation of transition in 3D flows originating from different walls. The formulation of the intermittency has also been extended to account for the rapid onset of transition caused by separation of the laminar boundary layer (Equ. 17). In addition the model can be fully calibrated with internal or proprietary transition onset and transition length correlations. The correlations can also be extended to flows with rough walls or to flows with cross-flow instability. It should be stressed that the proposed transport equations do not attempt to model the physics of the transition process (unlike e.g. turbulence models), but form a framework for the implementation of correlation-based models into general-purpose CFD methods. In order to distinguish the present concept from physics based transition modeling, it is named **LCTM** – Local Correlation-based Transition Modeling.

2.2 Transition model equations

The present transition model formulation is described very briefly for completeness, a detailed description of the model and its development can be found in Langtry et al. [25]. It should be noted that a few changes have been made to the model since it was first published [29] in order to improve the predictions of natural transition. These include:

- A new transition onset correlation that results in improved predictions for both natural and bypass transition.
- A modification to the separation induced transition modification that prevents it from causing early transition near the separation point.
- Some adjustments of the model coefficients in order to better account for flow history effects on the transition onset location.

It was expected that different groups will make numerous improvements to the model and consequently a naming convention was introduced in reference [29] in order to keep track of the various model versions. The basic model framework (transport equations without any correlations) was called the γ-Re$_θ$ transition model. The version number given in reference [29] was called CFX-v-1.0. Based on this naming convention, the present model with the above modifications will be referred to as the γ-Re$_θ$ model, CFX-v-1.1. The present transition model is briefly summarized in the following pages.

The transport equation for the intermittency, γ, reads:

$$\frac{\partial(\rho\gamma)}{\partial t} + \frac{\partial(\rho U_j \gamma)}{\partial x_j} = P_\gamma - E_\gamma + \frac{\partial}{\partial x_j}\left[\left(\mu + \frac{\mu_t}{\sigma_f}\right)\frac{\partial\gamma}{\partial x_j}\right]$$ (3)

The transition sources are defined as follows:

$$P_{\gamma 1} = F_{length} c_{a1} \rho S [\gamma F_{onset}]^{0.5} (1 - c_{e1}\gamma)$$ (4)

where S is the strain rate magnitude. F$_{length}$ is an empirical correlation that controls the length of the transition region. The destruction/relaminarization source is defined as follows:

$$E_\gamma = c_{a2} \rho \Omega \gamma F_{turb} (c_{e2}\gamma - 1)$$ (5)

where Ω is the vorticity magnitude. The transition onset is controlled by the following functions:

$$\mathrm{Re}_V = \frac{\rho y^2 S}{\mu}$$ (6)

$$F_{onset1} = \frac{\mathrm{Re}_v}{2.193 \cdot \mathrm{Re}_{\theta c}}$$ (7)

$$F_{onset2} = \min\left(\max\left(F_{onset1}, F_{onset1}^4\right), 2.0\right)$$ (8)

$$R_T = \frac{\rho k}{\mu\omega}$$ (9)

$$F_{onset3} = \max\left(1 - \left(\frac{R_T}{2.5}\right)^3, 0\right)$$ (10)

$$F_{onset} = \max\left(F_{onset2} - F_{onset3}, 0\right)$$ (11)

Re$_{θc}$ is the critical Reynolds number where the intermittency first starts to increase in the boundary layer. This occurs upstream of the transition Reynolds number, $\tilde{\mathrm{Re}}_{\theta t}$, and the difference between the two must be obtained from an empirical correlation. Both the F$_{length}$ and Re$_{θc}$ correlations are functions of $\tilde{\mathrm{Re}}_{\theta t}$.

Based on the T3B, T3A, T3A- and the Schubauer and Klebanof test cases a correlation for F_{length} based on $Re_{\theta t}$ from an empirical correlation is defined as:

$$F_{length} = \begin{cases} \left[398.189 \cdot 10^{-1} + (-119.270 \cdot 10^{-4})\tilde{Re}_{\theta t} + (-132.567 \cdot 10^{-6})\tilde{Re}_{\theta t}{}^2\right], \tilde{Re}_{\theta t} < 400 \\ \left[263.404 + (-123.939 \cdot 10^{-2})\tilde{Re}_{\theta t} + (194.548 \cdot 10^{-5})\tilde{Re}_{\theta t}{}^2 + (-101.695 \cdot 10^{-8})\tilde{Re}_{\theta t}{}^3\right], 400 \leq \tilde{Re}_{\theta t} < 596 \\ \left[0.5 - \left(\tilde{Re}_{\theta t} - 596.0\right) \cdot 3.0 \cdot 10^{-4}\right], 596 \leq \tilde{Re}_{\theta t} < 1200 \\ \left[0.3188\right], 1200 \leq \tilde{Re}_{\theta t} \end{cases} \quad (12)$$

In certain cases such as transition at higher Reynolds numbers the transport equation for $\tilde{Re}_{\theta t}$ will often decrease to very small values in the boundary layer shortly after transition. Because F_{length} is based on $\tilde{Re}_{\theta t}$ this can result in a local increase in the source term for the intermittency equation, which in turn can show up as a sharp increase in the skin friction. The skin friction does eventually return back to the fully turbulent value however this effect is unphysical. It appears to be caused by a sharp change in the y+ in the viscous sublayer where the intermittency decreases back to its minimum value due to the destruction term (Eq. 5). The effect can be eliminated by forcing F_{length} to always be equal to its maximum value (in this case 40.0) in the viscous sublayer. The modification for doing this is shown below. The modification does not appear to have any effect on the predicted transition length. An added benefit is that at higher Reynolds numbers the model now appears to predict the skin friction over shoot measured by experiments.

$$F_{sublayer} = e^{-\left(\frac{R_\omega}{0.4}\right)^2} \quad (13)$$

$$R_\omega = \frac{\rho y^2 \omega}{500 \mu} \quad (14)$$

$$F_{length} = F_{length}\left(1 - F_{sublayer}\right) + 40.0 \cdot F_{sublayer} \quad (15)$$

The correlation between $Re_{\theta c}$ and $\tilde{Re}_{\theta t}$ is defined as follows:

$$Re_{\theta c} = \begin{cases} \left[\tilde{Re}_{\theta t} - \left(\begin{array}{c} 396.035 \cdot 10^{-2} + (-120.656 \cdot 10^{-4})\tilde{Re}_{\theta t} + (868.230 \cdot 10^{-6})\tilde{Re}_{\theta t}{}^2 \\ + (-696.506 \cdot 10^{-9})\tilde{Re}_{\theta t}{}^3 + (174.105 \cdot 10^{-12})\tilde{Re}_{\theta t}{}^4 \end{array}\right)\right], \tilde{Re}_{\theta t} \leq 1870 \\ \left[\tilde{Re}_{\theta t} - \left(593.11 + \left(\tilde{Re}_{\theta t} - 1870.0\right) \cdot 0.482\right)\right], \tilde{Re}_{\theta t} > 1870 \end{cases} \quad (16)$$

The constants for the intermittency equation are:

$$c_{e1} = 1.0; \quad c_{a1} = 2.0; \qquad c_{e2} = 50; \quad c_{a2} = 0.06; \quad \sigma_f = 1.0;$$

The modification for separation-induced transition is:

$$\gamma_{sep} = \min\left(s_1 \max\left[0, \left(\frac{Re_v}{3.235 Re_{\theta c}}\right) - 1\right] F_{reattach}, 2\right) F_{\theta t} \quad (17)$$

$$F_{reattach} = e^{-\left(\frac{R_T}{20}\right)^4} \qquad (18)$$

$$\gamma_{eff} = \max\left(\gamma, \gamma_{sep}\right) \qquad (19)$$

$$s_1 = 2 \qquad (20)$$

The model constants in Equ. 17 have been adjusted from those of Menter et al. [31] in order to improve the predictions of separated flow transition. See Langtry [33] for a detailed discussion of the changes to the model from the Menter et al. [31] version. The main difference is the constant that controls the relation between Re_v and $Re_{\theta c}$ was changed from 2.193, it's value for a Blasius boundary layer, to 3.235, the value at a separation point where the shape factor (H) is 3.5 (see Figure 2). The boundary condition for γ at a wall is zero normal flux while for an inlet γ is equal to 1.0. An inlet γ equal to 1.0 is necessary in order to preserve the original turbulence models freestream turbulence decay rate.

The transport equation for the transition momentum thickness Reynolds number, $\tilde{Re}_{\theta t}$, reads:

$$\frac{\partial\left(\rho\tilde{Re}_{\theta t}\right)}{\partial t} + \frac{\partial\left(\rho U_j \tilde{Re}_{\theta t}\right)}{\partial x_j} = P_{\theta t} + \frac{\partial}{\partial x_j}\left[\sigma_{\theta t}\left(\mu + \mu_t\right)\frac{\partial \tilde{Re}_{\theta t}}{\partial x_j}\right] \qquad (21)$$

Outside the boundary layer, the source term $P_{\theta t}$ is designed to force the transported scalar $\tilde{Re}_{\theta t}$ to match the local value of $Re_{\theta t}$ calculated from the empirical correlation (Equ. 35, 36). The source term is defined as follows:

$$P_{\theta t} = c_{\theta t}\frac{\rho}{t}\left(Re_{\theta t} - \tilde{Re}_{\theta t}\right)\left(1.0 - F_{\theta t}\right) \qquad (22)$$

$$t = \frac{500\mu}{\rho U^2} \qquad (23)$$

where t is a time scale, which is present for dimensional reasons. The time scale was determined based on dimensional analysis with the main criteria being that it had to scale with the convective and diffusive terms in the transport equation. The blending function $F_{\theta t}$ is used to turn off the source term in the boundary layer and allow the transported scalar $\tilde{Re}_{\theta t}$ to diffuse in from the freestream. $F_{\theta t}$ is equal to zero in the freestream and one in the boundary layer. The $F_{\theta t}$ blending function is defined as follows:

$$F_{\theta t} = \min\left(\max\left(F_{wake}\cdot e^{-\left(\frac{y}{\delta}\right)^4}, 1.0 - \left(\frac{\gamma - 1/c_{e2}}{1.0 - 1/c_{e2}}\right)^2\right), 1.0\right) \qquad (24)$$

$$\theta_{BL} = \frac{\tilde{Re}_{\theta t}\mu}{\rho U}; \quad \delta_{BL} = \frac{15}{2}\theta_{BL}; \quad \delta = \frac{50\Omega y}{U}\cdot\delta_{BL} \qquad (25)$$

$$\mathrm{Re}_\omega = \frac{\rho \omega y^2}{\mu}; \quad F_{wake} = e^{-\left(\frac{\mathrm{Re}_\omega}{1E+5}\right)^2} \tag{26}$$

The F_{wake} function ensures that the blending function is not active in the wake regions downstream of an airfoil/blade.

The model constants for the $\tilde{\mathrm{Re}}_{\theta t}$ equation are:

$$c_{\theta t} = 0.03; \quad \sigma_{\theta t} = 2.0 \tag{27}$$

The boundary condition for $\tilde{\mathrm{Re}}_{\theta t}$ at a wall is zero flux. The boundary condition for $\tilde{\mathrm{Re}}_{\theta t}$ at an inlet should be calculated from the empirical correlation (Equ. 35, 36) based on the inlet turbulence intensity.

The empirical correlation for transition onset is based on the following parameters:

$$\lambda_\theta = \frac{\rho \theta^2}{\mu} \frac{dU}{ds} \tag{28}$$

$$Tu = 100 \frac{\sqrt{2k/3}}{U} \tag{29}$$

Where dU/ds is the acceleration along the streamwise direction and can be computed by taking the derivative of the velocity (U) in the x, y and z directions and then summing the contribution of these derivatives along the streamwise flow direction:

$$U = \left(u^2 + v^2 + w^2\right)^{\frac{1}{2}} \tag{30}$$

$$\frac{dU}{dx} = \frac{1}{2}\left(u^2 + v^2 + w^2\right)^{-\frac{1}{2}} \cdot \left[2u\frac{du}{dx} + 2v\frac{dv}{dx} + 2w\frac{dw}{dx}\right] \tag{31}$$

$$\frac{dU}{dy} = \frac{1}{2}\left(u^2 + v^2 + w^2\right)^{-\frac{1}{2}} \cdot \left[2u\frac{du}{dy} + 2v\frac{dv}{dy} + 2w\frac{dw}{dy}\right] \tag{32}$$

$$\frac{dU}{dz} = \frac{1}{2}\left(u^2 + v^2 + w^2\right)^{-\frac{1}{2}} \cdot \left[2u\frac{du}{dz} + 2v\frac{dv}{dz} + 2w\frac{dw}{dz}\right] \tag{33}$$

$$\frac{dU}{ds} = \left[(u/U)\frac{dU}{dx} + (v/U)\frac{dU}{dy} + (w/U)\frac{dU}{dz}\right] \tag{34}$$

The use of the streamline direction is not Galilean invariant. However, this deficiency is inherent to all correlation-based models, as their main variable, the turbulence intensity is already based on the local freestream velocity and does therefore violate Galilean invariance. This is not problematic, as the correlations are defined with respect to a wall boundary layer and all velocities are therefore relative to the wall. Nevertheless, multiple moving walls in one domain will likely require additional information.

The use of the streamline direction is not Galilean invariant. However, this deficiency is inherent to all correlation-based models, as their main variable, the turbulence intensity is already based on the local freestream velocity and does therefore violate Galilean invariance. This is not problematic, as the correlations are defined with respect to a wall boundary layer and all velocities are therefore relative to the wall. Nevertheless, multiple moving walls in one domain will likely require additional information.

The empirical correlation has been modified from reference [29] to improve the predictions of natural transition. The predicted transition Reynolds number as a function of turbulence intensity is shown in Figure 3. For pressure gradient flows the model predictions are similar to the Abu-Ghannam and Shaw [17] correlation. The empirical correlation is defined as follows:

$$\mathrm{Re}_{\theta t} = \left[1173.51 - 589.428 Tu + \frac{0.2196}{Tu^2}\right] F(\lambda_\theta), Tu \le 1.3 \tag{35}$$

$$\mathrm{Re}_{\theta t} = 331.50 [Tu - 0.5658]^{-0.671} F(\lambda_\theta), Tu > 1.3 \tag{36}$$

$$F(\lambda_\theta) = 1 - \left[-12.986\lambda_\theta - 123.66\lambda_\theta^2 - 405.689\lambda_\theta^3\right] e^{-\left[\frac{Tu}{1.5}\right]^{1.5}}, \lambda_\theta \le 0 \tag{37}$$

$$F(\lambda_\theta) = 1 + 0.275 \left[1 - e^{[-35.0\lambda_\theta]}\right] e^{\left[\frac{-Tu}{0.5}\right]}, \lambda_\theta > 0 \tag{38}$$
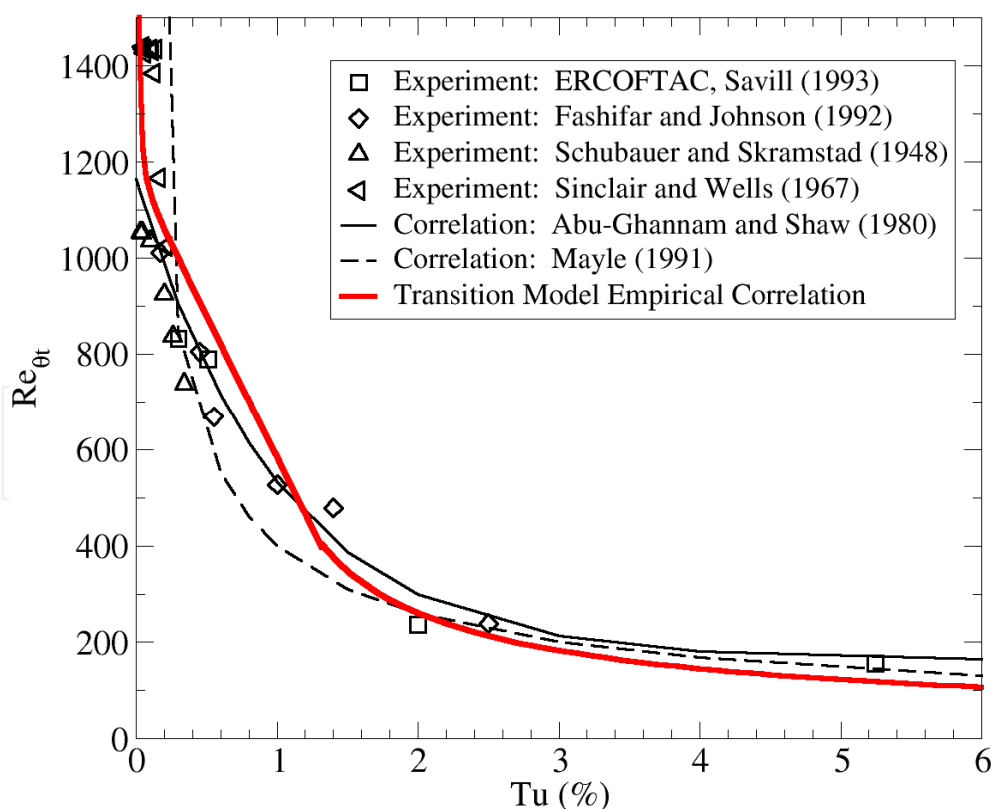
Fig. 3. Transition onset momentum thickness Reynolds number ($\mathrm{Re}_{\theta t}$) predicted by the new correlation as a function of turbulence intensity (Tu) for a flat plate with zero pressure gradient.

For numerical robustness the acceleration parameters, the turbulence intensity and the empirical correlation should be limited as follows:

$$-0.1 \leq \lambda_{\theta} \leq 0.1$$

$$Tu \geq 0.027$$

$$\mathrm{Re}_{\theta t} \geq 20$$

A minimum turbulence intensity of 0.027 percent results in a transition momentum thickness Reynolds number of 1450, which is the largest experimentally observed flat plate transition Reynolds number based on the Sinclair and Wells [36] data. For cases where larger transition Reynolds are believed to occur (e.g. aircraft in flight) this limiter may need to be adjusted downwards.

The empirical correlation is used only in the source term (Eq. 22) of the transport equation for the transition onset momentum thickness Reynolds number. Equations 35 to 38 must be solved iteratively because the momentum thickness (θ_t) is present in the left hand side of the equation and also in the right hand side in the pressure gradient parameter (λ_{θ}). In the present work an initial guess for the local value of θ_t was obtained based on the zero pressure gradient solution of Eq. 35, 36 and the local values of U, ρ and μ. With this initial guess, equations 35 to 38 were solved by iterating on the value of θ_t and convergence was obtained in less then ten iterations using a shooting point method.

The transition model interacts with the SST turbulence model [32], as follows:

$$\frac{\partial}{\partial t}(\rho k) + \frac{\partial}{\partial x_j}(\rho u_j k) = \tilde{P}_k - \tilde{D}_k + \frac{\partial}{\partial x_j}\left(\left(\mu + \sigma_k \mu_t \right) \frac{\partial k}{\partial x_j} \right) \tag{39}$$

$$\tilde{P}_k = \gamma_{eff} P_k; \quad \tilde{D}_k = \min\left(\max(\gamma_{eff}, 0.1), 1.0 \right) D_k \tag{40}$$

$$R_y = \frac{\rho y \sqrt{k}}{\mu}; \quad F_3 = e^{-\left(\frac{R_y}{120} \right)^8}; \quad F_1 = \max\left(F_{1orig}, F_3 \right) \tag{41}$$

where P_k and D_k are the original production and destruction terms for the SST model and F_{1orig} is the original SST blending function. Note that the production term in the ω-equation is not modified. The rationale behind the above model formulation is given in detail in reference [29].

In order to capture the laminar and transitional boundary layers correctly, the grid must have a y^+ of approximately one at the first grid point off the wall. If the y^+ is too large (i.e. > 5) then the transition onset location moves upstream with increasing y^+. All simulations have been performed with CFX-5 using a bounded second order upwind biased discretisation for the mean flow, turbulence and transition equations.

3. Test cases

The remaining part of the chapter will give an overview of some of the public-domain testcases which have been computed with the model described above. This naturally

requires a compact representation of the simulations. Most of the cases are described in far more detail in reference [33], including grid refinement and sensitivity studies.

3.1 Flat plate test cases

The flat plate test cases that where used to calibrate the model are the ERCOFTAC T3 series of flat plate experiments [12, 13] and the Schubauer and Klebanof [37] flat plate experiment, all of which are commonly used as benchmarks for transition models. Also included is a test case where the boundary layer experiences a strong favorable pressure gradient that causes it to relaminarize [38]. The inlet conditions for these testcases are summarized in Table 1.

The three cases T3A-, T3A, and T3B have zero pressure gradients with different freestream turbulence intensity (FSTI) levels corresponding to transition in the bypass regime. The Schubauer and Klebanof (S&K) test case has a low free-stream turbulence intensity and corresponds to natural transition. Figure 4 shows the comparison of the model prediction with experimental data for theses cases. It also gives the corresponding FSTI values. In all simulations, the inlet turbulence levels were specified to match the experimental turbulence intensity and its decay rate. This was done by fixing the inlet turbulence intensity and via trial and error adjusting the inlet viscosity ratio (i.e. the ω inlet condition) to match the experimentally measured turbulence levels at various downstream locations. As the freestream turbulence increases, the transition location moves to lower Reynolds numbers.
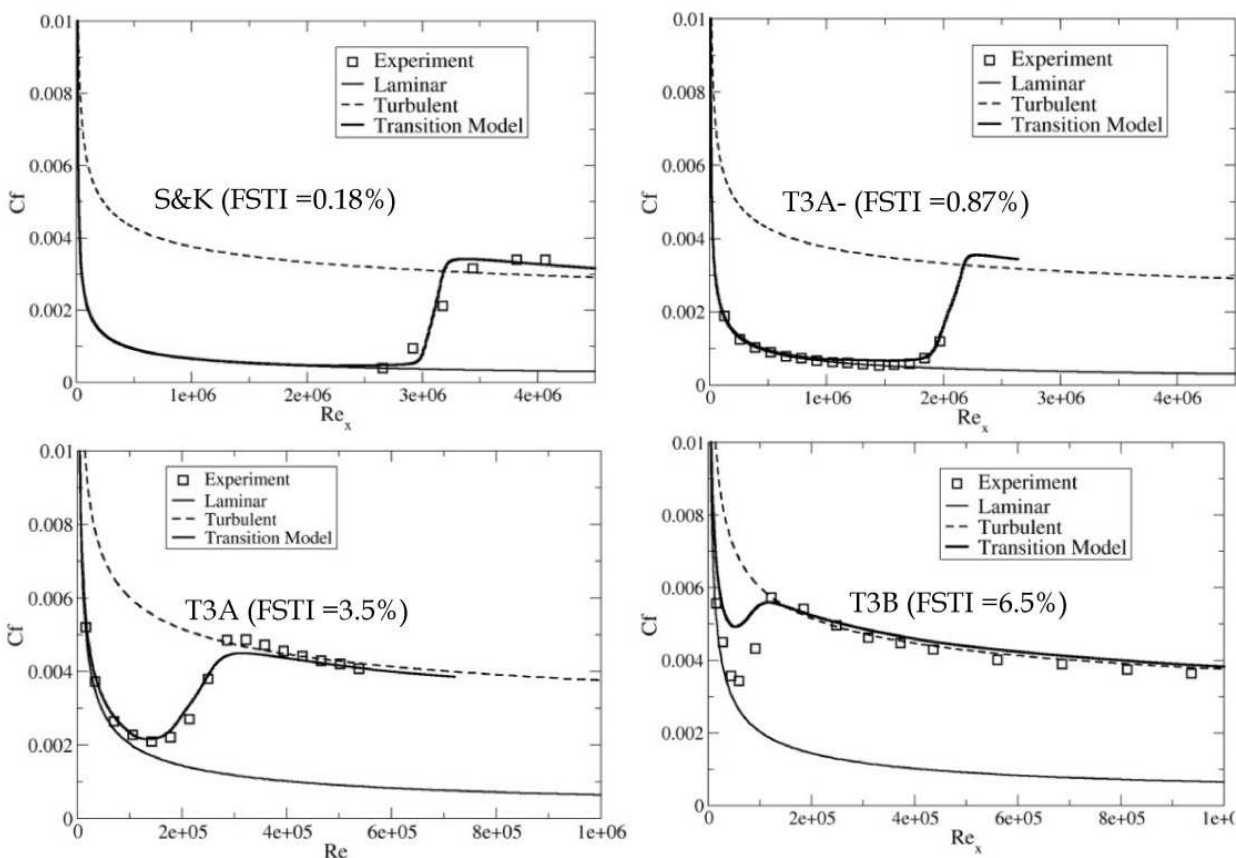
Fig. 4. Results for flat plate test cases with different freestream turbulence levels (FSTI – Freestream Turbulence Intensity).

Case	Inlet Velocity (m/s)	Turbulence Intensity (%) Inlet / Leading Edge value	μ_t / μ	Density (kg/m³)	Dynamic Viscosity (kg/ms)
T3A	5.4	3.3	12.0	1.2	1.8×10^{-5}
T3B	9.4	6.5	100.0	1.2	1.8×10^{-5}
T3A-	19.8	0.874	8.72	1.2	1.8×10^{-5}
Schubauer and Klebanof	50.1	0.3	1.0	1.2	1.8×10^{-5}
T3C2	5.29	3.0	11.0	1.2	1.8×10^{-5}
T3C3	4.0	3.0	6.0	1.2	1.8×10^{-5}
T3C4	1.37	3.0	8.0	1.2	1.8×10^{-5}
T3C5	9.0	4.0	15.0	1.2	1.8×10^{-5}
Relaminarization	1.4	5.5	15	1.2	1.8×10^{-5}

Table 1. Inlet condition for the flat plate test cases.

The T3C test cases consist of a flat plate with a favorable and adverse pressure gradient imposed by the opposite converging/diverging wall. The wind tunnel Reynolds number was varied for the four cases (T3C5, T3C3, T3C2, T3C4) thus moving the transition location from the favorable pressure at the beginning of the plate to the adverse pressure gradient at the end. The cases are used to demonstrate the transition models ability to predict transition under the influence of various pressure gradients. Figure 5 details the results for the
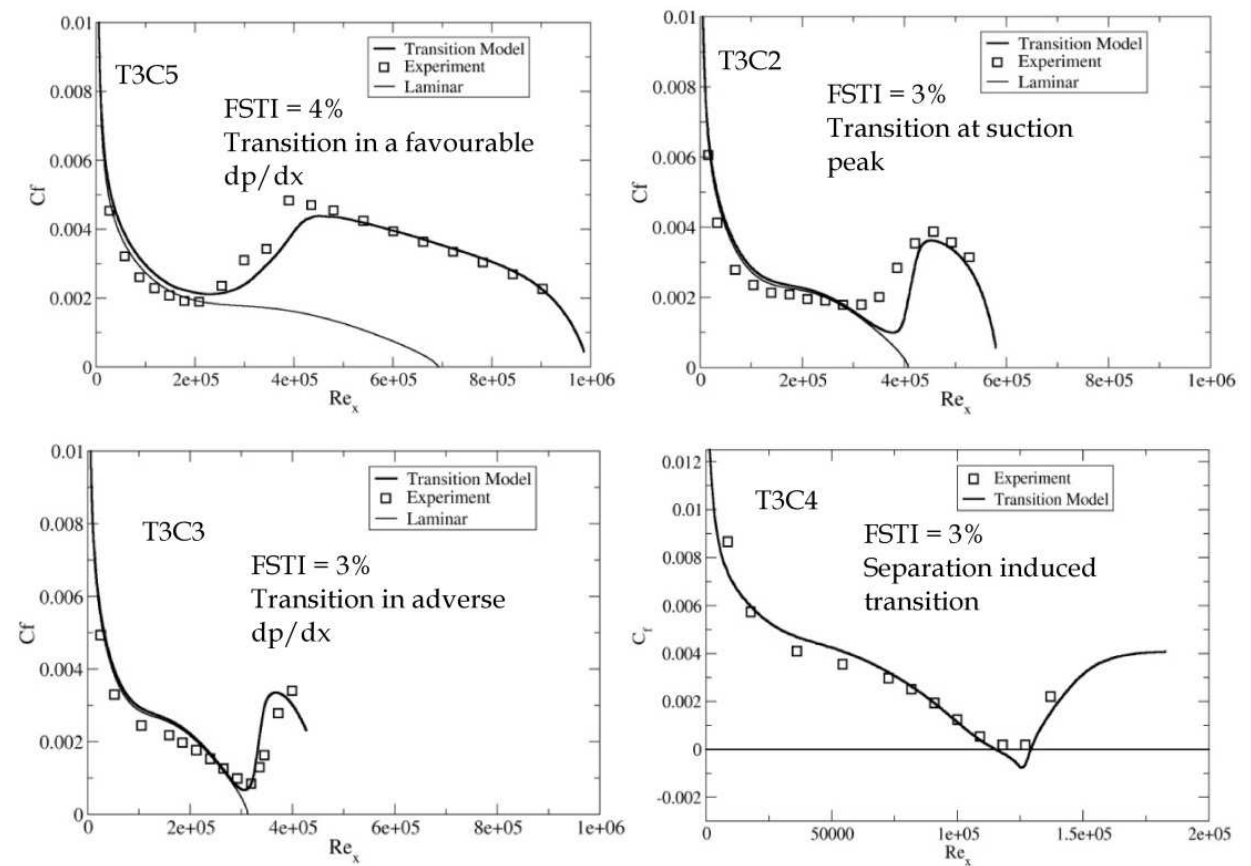
Fig. 5. Results for flat plate test cases where variation of the tunnel Reynolds number causes transition to occur in different pressure gradients (dp/dx).

pressure gradient cases. The effect of the pressure gradient on the transition length is clearly visible with favorable pressure gradients increasing the transition length and adverse pressure gradients reducing it. For the T3C4 case the laminar boundary layer actually separates and undergoes separation induced transition.

The relaminarization test case is shown in Figure 6. For this case the opposite converging wall imposes a strong favorable pressure gradient that can relaminarize a turbulent boundary layer. In both the experiment and in the CFD prediction the boundary layer was tripped near the plate leading edge. In the CFD computation this was accomplished by injecting a small amount of turbulent air into the boundary layer with a turbulence intensity of 3%. The same effect could have been accomplished with a small step or gap in the CFD geometry. Downstream of the trip the boundary layer slowly relaminarizes due to the strong favorable pressure gradient.

For all of the flat plate test cases the agreement with the data is generally good, considering the diverse nature of the physical phenomena computed, ranging from bypass transition to natural transition, separation-induced transition and even relaminarization.
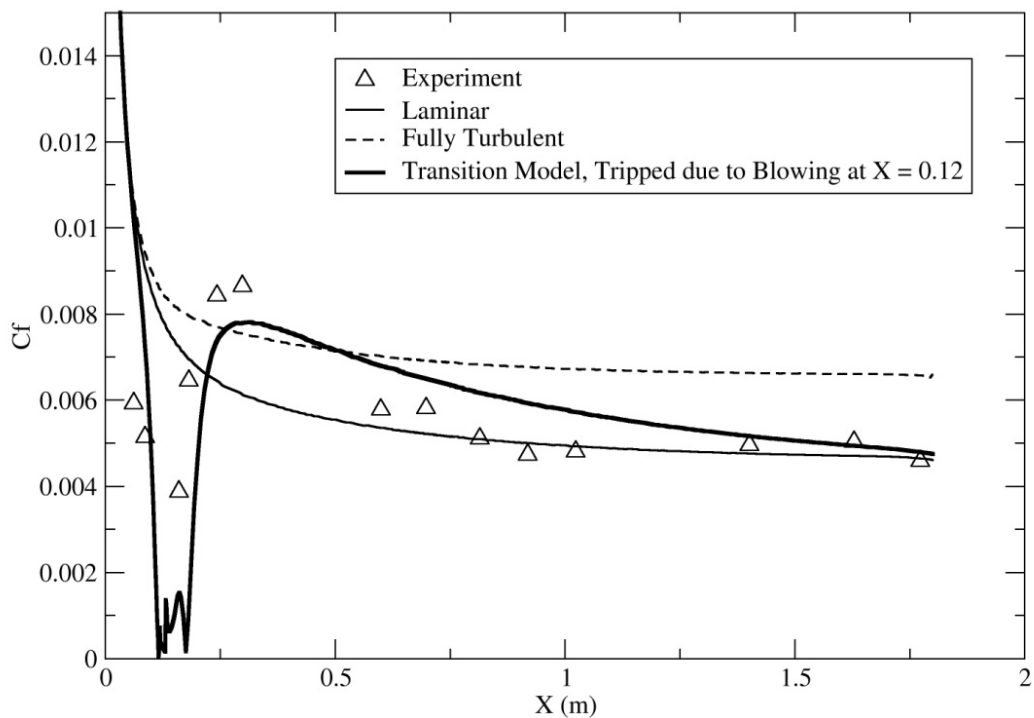
Fig. 6. Predicted skin friction (Cf) for a flat plate with a strong acceleration that causes the boundary layer to relaminarize.

3.2 Turbomachinery test cases

This section descrives a few of the turbomachinery test cases that have been used to validate the transition model including a compressor blade, a low-pressure turbine and a high pressure turbine. A summary of the inlet conditions is shown in Table 2.

For the Zierke and Deutsch [39] compressor blade, transition on the suction side occurs at the leading edge due to a small leading edge separation bubble on the suction side. On the pressure side, transition occurs at about mid-chord. The turbulence contours and the skin

Case	$Re_x = \rho c U_o / \mu$ (x10^6)	Mach $= U_o / a$ where speed of sound (a) $= (\gamma RT)^{0.5}$	Chord (c) (m)	FSTI (%)	μ_t / μ
Zierke and Deutsch Compressor Incidence = -1.5°	0.47	0.1	0.2152	0.18	2.0
Pak-B Low-Pressure Turbine Blade	0.05, 0.075, 0.1	0.03	0.075	0.08, 2.35, 6.0	6.5 - 30
VKI MUR Transonic Guide Vane	0.26	Inlet: 0.15 Outlet: 1.06	0.037	1.0, 6.5	11, 1000

Table 2. Inlet conditions for the turbomachinery test cases.

friction distribution are shown in Figure 7. There appears to be a significant amount of scatter in the experimental data; however, overall the transition model is predicting the major flow features correctly (i.e. fully turbulent suction side, transition at mid-chord on the pressure side). One important issue to note is the effect of stream-wise grid resolution on resolving the leading edge laminar separation and subsequent transition on the suction side. If the number of stream-wise nodes clustered around the leading edge is too low, the model cannot resolve the rapid transition and a laminar boundary layer on the suction side is the result. For the present study, 60 streamwise nodes were used between the leading edge and the x/C = 0.1 location.

The Pratt and Whitney PAK-B low pressure turbine blade is a particularly interesting airfoil because it has a loading profile similar to the rotors found in many modern aircraft engines [40]. The low-pressure rotors on modern aircraft engines are extremely challenging flow fields. This is because in many cases the transition occurs in the free shear layer of a separation bubble on the suction side [4]. The onset of transition in the free shear layer determines whether or not the separation bubble will reattach as a turbulent boundary layer and, ultimately, whether or not the blade will stall. The present transition model would therefore be of great interest to turbine designers if it can accurately predict the transition onset location for these types of flows.

Huang et al. [41] conducted experiments on the PAK-B blade cascade for a range of Reynolds numbers and turbulence intensities. The experiments were performed at the design incidence angle for Reynolds numbers of 50,000, 75,000, and 100,000 based on inlet velocity and axial chord length, with turbulence intensities of 0.08%, 2.35% and 6.0% (which corresponded to values of 0.08%, 1.6%, and 2.85% at the leading edge of the blade). The computed pressure coefficient distributions obtained with the transition model and fully turbulent model are compared to the experimental data for the 75 000 Reynolds number, 2.35% turbulent intensity case in Figure 8. On the suction side, a pressure plateau due to a laminar separation with turbulent reattachment exists. The fully turbulent computation completely misses this phenomenon because the boundary layer remains attached over the entire length of the suction surface. The transition model can predict the pressure plateau due to the laminar separation and the subsequent turbulent reattachment location. The pressure side was predicted to be fully attached and laminar.
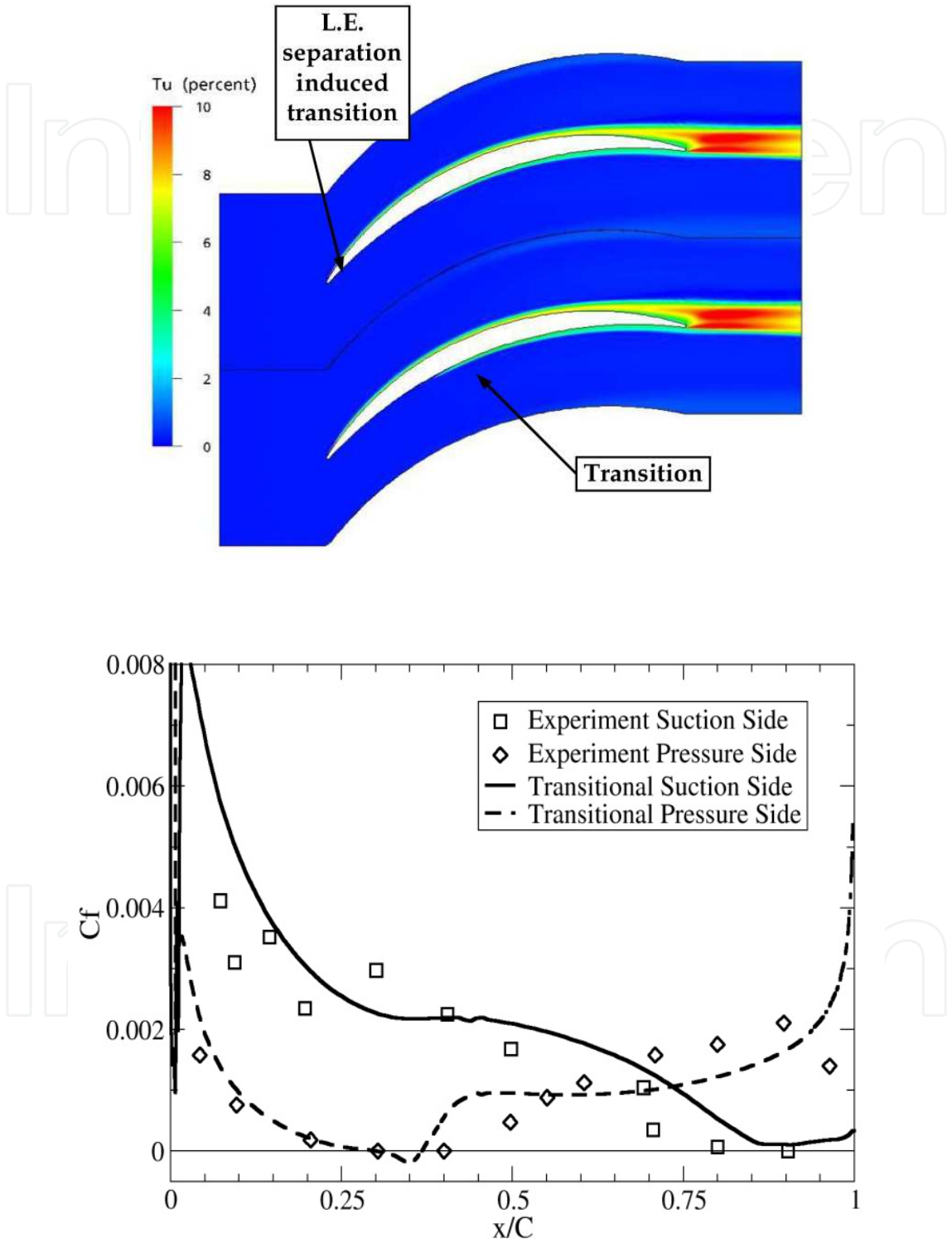
Fig. 7. Turbulence intensity contours (top) and cf-distribution against experimental data (right) for the Zierke & Deutsch compressor.
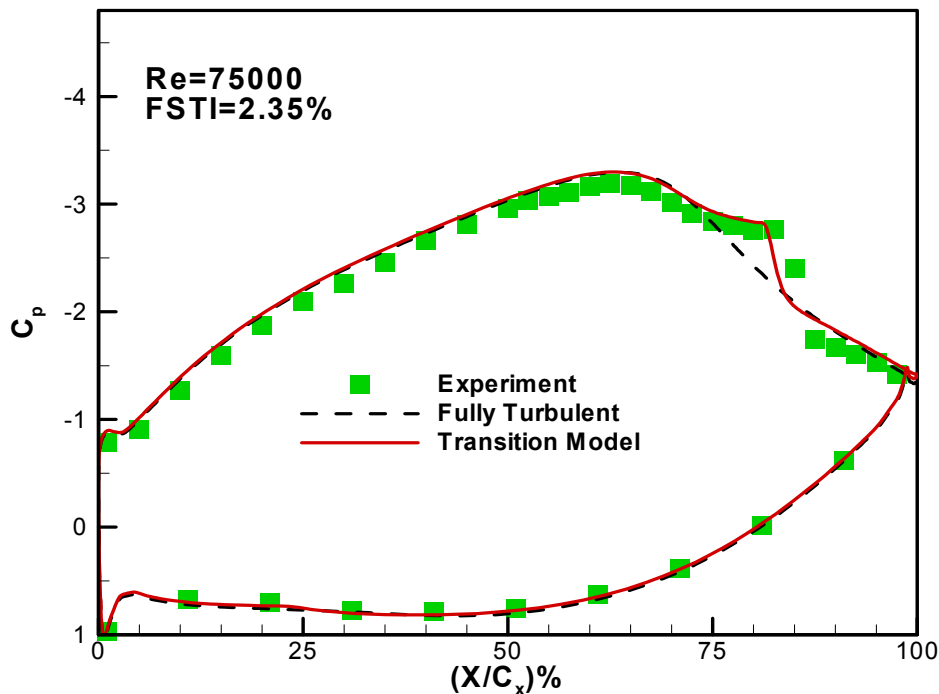
Fig. 8. Predicted blade loading for the Pak-B Low-Pressure turbine at a Reynolds number of 75 000 and a freestream turbulent intensity (FSTI) of 2.35%.

The computed pressure coefficient distributions for various Reynolds numbers and freestream turbulence intensities compared to experimental data are shown in Figure 9. In this figure, the comparisons are organized such that the horizontal axis denotes the Reynolds number whereas the vertical axis corresponds to the freestream turbulence intensity of the specific case. As previously pointed out, the most important feature of this test case is the extent of the separation bubble on the suction side, characterized by the plateau in the pressure distribution. The size of the separation bubble is actually a complex function of the Reynolds number and the freestream turbulence value. As the Reynolds number or freestream turbulence decrease, the size of the separation and hence the pressure plateau increases. The computations with the transition model compare well with the experimental data for all of the cases considered, illustrating the ability of the model to capture the effects of Reynolds number and turbulence intensity variations on the size of a laminar separation bubble and the subsequent turbulent reattachment.

The surface heat transfer for the transonic VKI MUR 241 (FSTI = 6.0%) and MUR 116 (FSTI = 1.0%) test cases [42] is shown in Figure 10. The strong acceleration on the suction side for the MUR 241 case keeps the flow laminar until a weak shock at mid chord, whereas for the MUR 116 case the flow is laminar until right before the trailing edge. Downstream of transition there appears to be a significant difference between the predicted turbulent heat transfer and the measured value. It is possible that this is the result of a Mach number (inlet Mach number Ma_{inlet}=0.15, Ma_{outlet}=1.089) effect on the transition length [43]. At present, no attempt has been made to account for this effect in the model. It can be incorporated in future correlations, if found consistently important.
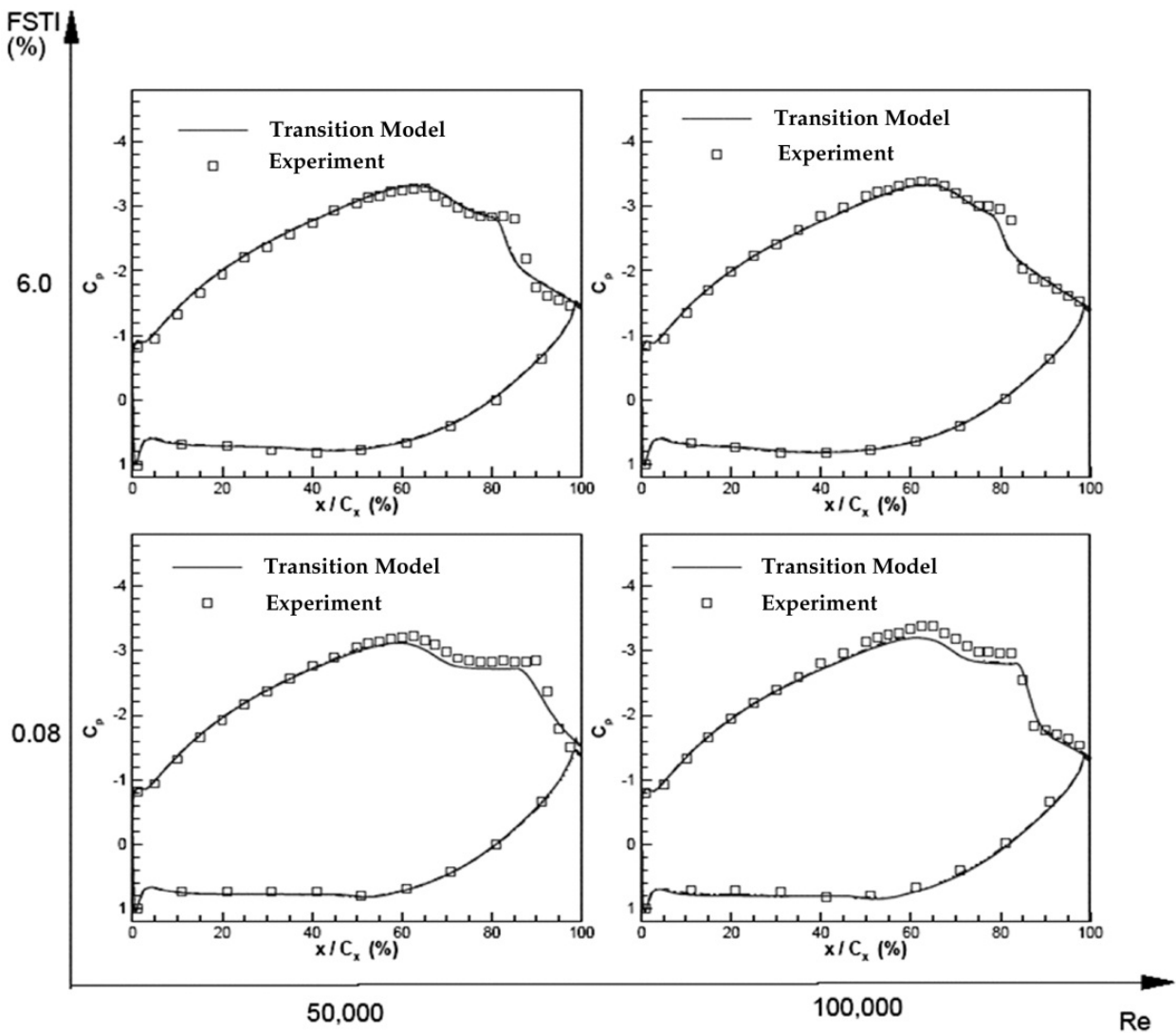
Fig. 9. Blade loading for the Pak-B Low-Pressure turbine at various freestream turbulence intensities (FSTI) and Reynolds numbers (Re).

The pressure side heat transfer is of particular interest for this case. For both cases, transition did not occur on the pressure side, however, the heat transfer was significantly increased for the high turbulence intensity case. This is a result of the large freestream levels of turbulence which diffuse into the laminar boundary layer and increase the heat transfer and skin friction. From a modeling standpoint, the effect was caused by the large freestream viscosity ratio necessary for MUR 241 to keep the turbulence intensity from decaying below 6%, which is the freestream value quoted in the experiment. The enhanced heat transfer on the pressure side was also present in the experiment and the effect appears to be physical. The model can predict this effect, as the intermittency does not multiply the eddy-viscosity but only the production term of the k-equation. The diffusive terms are therefore active in the laminar region.

The S809 airfoil is a 21% thick, laminar-flow airfoil that was designed specifically for horizontal-axis wind turbine (HAWT) applications. The airfoil profile is shown in Figure 11. The experimental results where obtained in the low-turbulence wind tunnel at the Delft
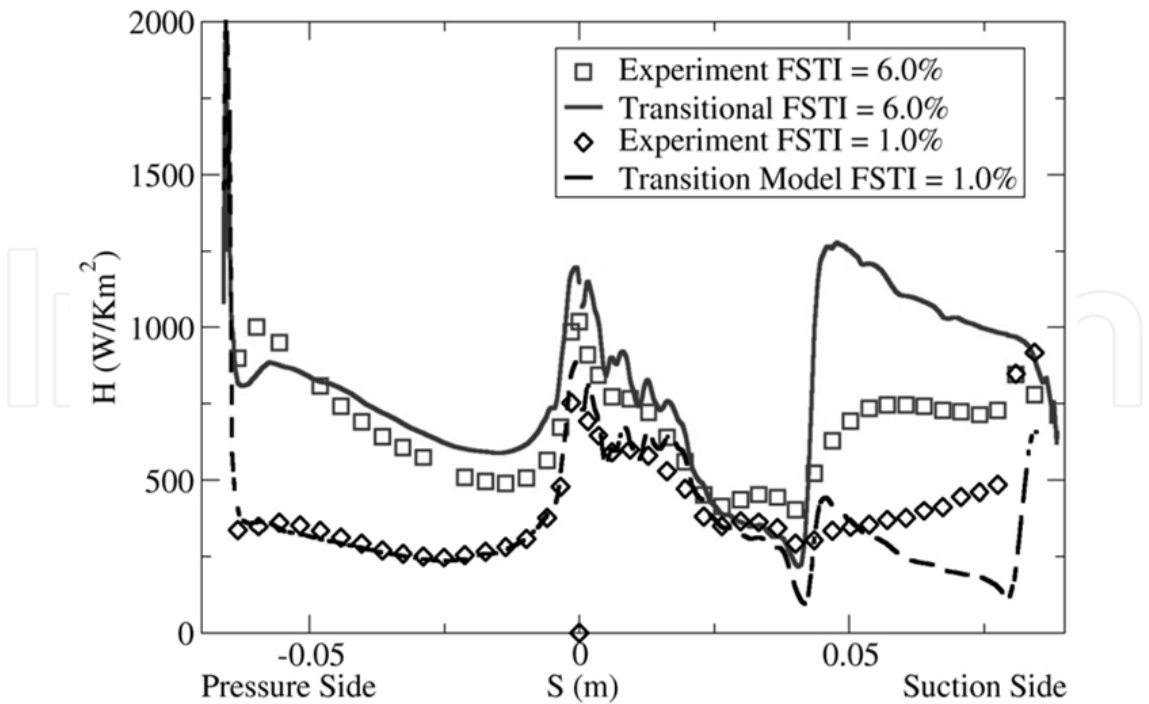
Fig. 10. Heat transfer for the VKI MUR241 (FSTI = 6.0%) and MUR116 (FSTI = 1.0%) test cases.
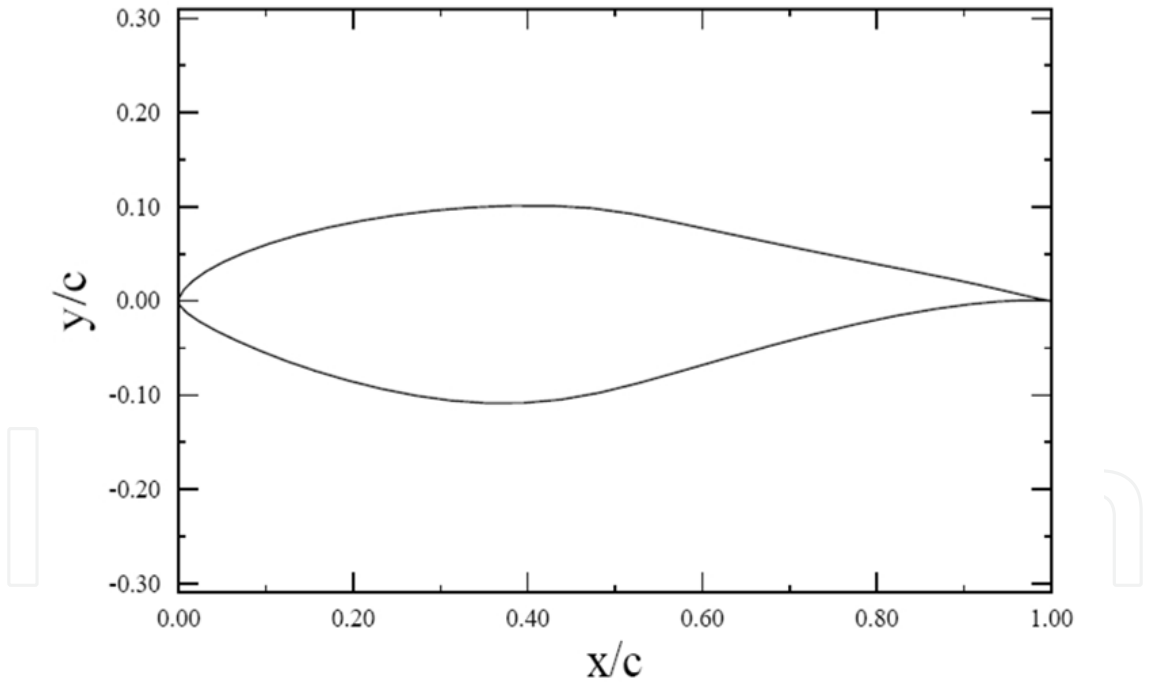
Fig. 11. S809 Airfoil Profile.

University of Technology [44, 45]. The detailed CFD results can be found in reference [46]. The predicted pressure distribution around the airfoil for angles of attack (AoA) of 1° is shown in Figure 12. For the 1° AoA case the flow is laminar for the first 0.5 chord of the airfoil on both the suction and pressure sides. The boundary layers then undergo a laminar separation and reattach as a turbulent boundary layer and this is clearly visible in the experimental pressure distribution plateaus. The fully turbulent computation obviously
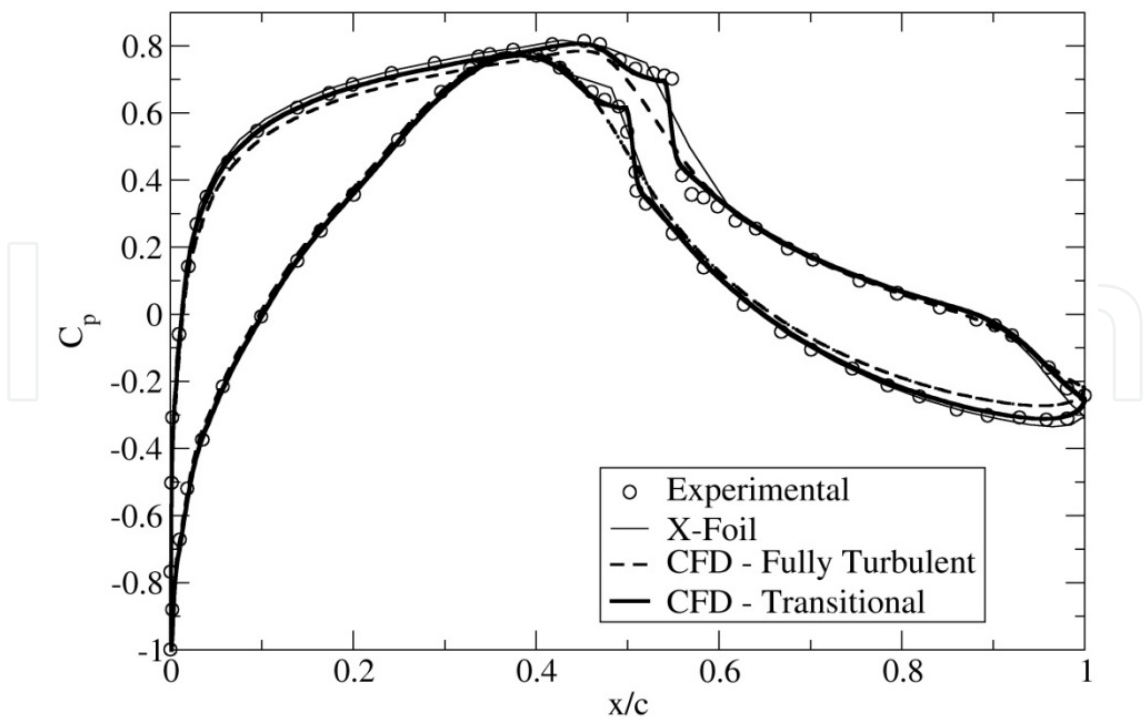
Fig. 12. Pressure distribution (Cp) for the S809 airfoil at 1° angle of attack.

does not capture this phenomenon, as the turbulent boundary layers remain completely attached. Both the transitional CFD and X-Foil solutions do predict the laminar separation bubble. However, X-Foil appears to slightly over predict the reattachment location while the transitional CFD simulation is in very good agreement with the experiment.

Case	Re_x (x10^6)	Mach	Chord (m)	FSTI (%)	μ_t/μ
S809 Airfoil	2.0	0.1	1	0.2	10

Table 3. Inlet conditions for the S809 test case.

The predicted transition locations as a function of angle of attack are shown in Figure 13. The experimental transition locations were obtained using a stethoscope method (Somers, [42]). In general the present transition model would appear to be in somewhat better agreement with the experiment than the X-Foil code, particularly around 14° angle of attack. However, at the moderate angles of attack all of the results appear be to within approximately 5% chord of each other. The X-Foil transition locations appear to change quite rapidly over a few degrees angle of attack while the transition model has a much smoother change in the transition location. The experimental data would appear to confirm that the smooth change in transition location is more physical, however this observation is based primarily on the 10° and 14° angle of attack cases. The results obtained for the lift and drag polars are shown in Figures 14 and 15. Between 0° and 9° the lift coefficients (Cl) predicted by the transitional CFD results are in very good agreement with the experiment while both the XFoil and fully turbulent CFD and results appear to under-predict the lift curve by approximately 0.1. As well, between 0° and 9° the drag coefficient (Cd) predicted by the transitional CFD and X-Foil results are in very good agreement with the experiment while the fully turbulent CFD simulation significantly over predicts the drag, as expected.
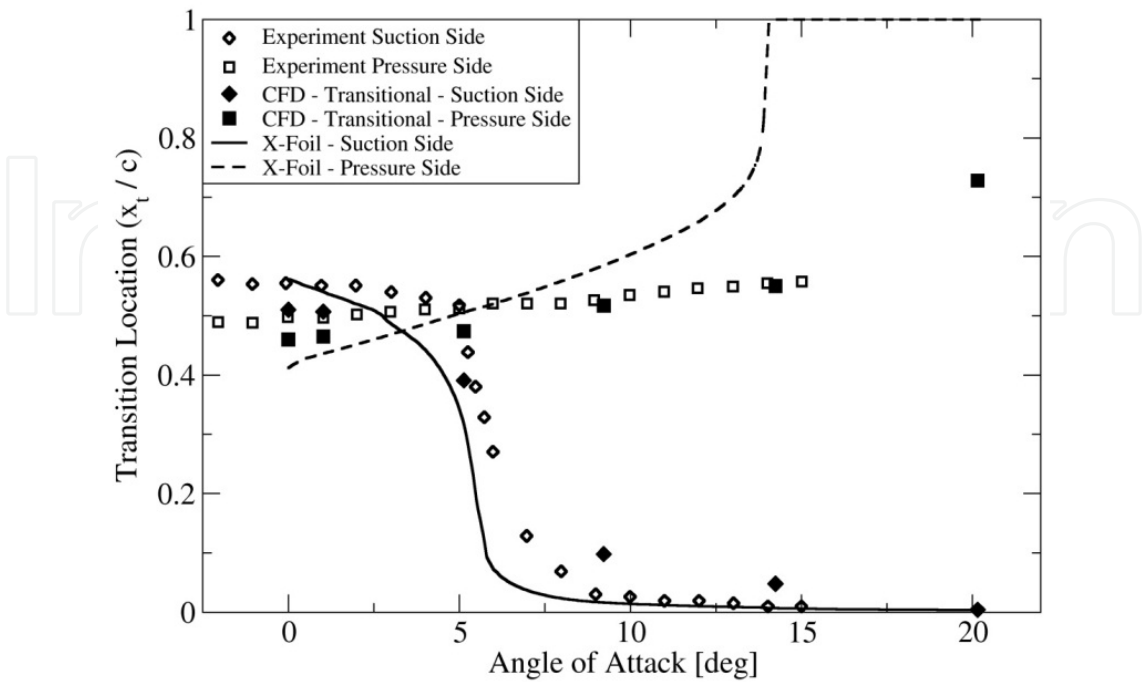
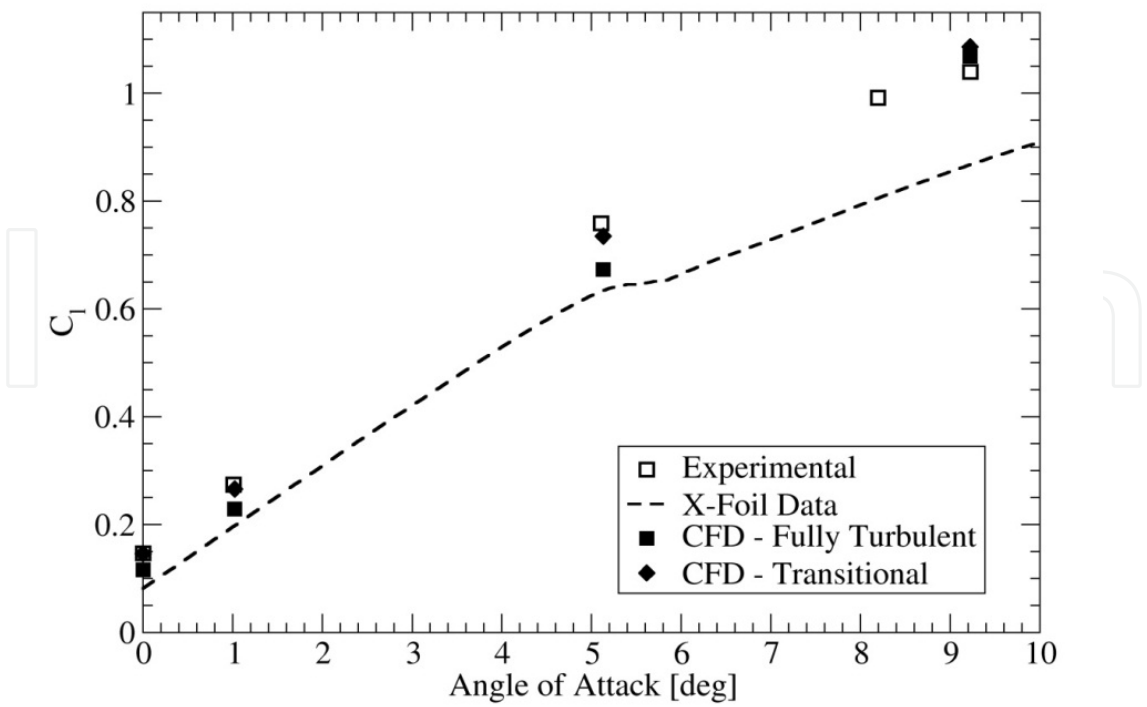Fig. 13. Transition location (xt/c) vs angle of attack for the S809 airfoil.

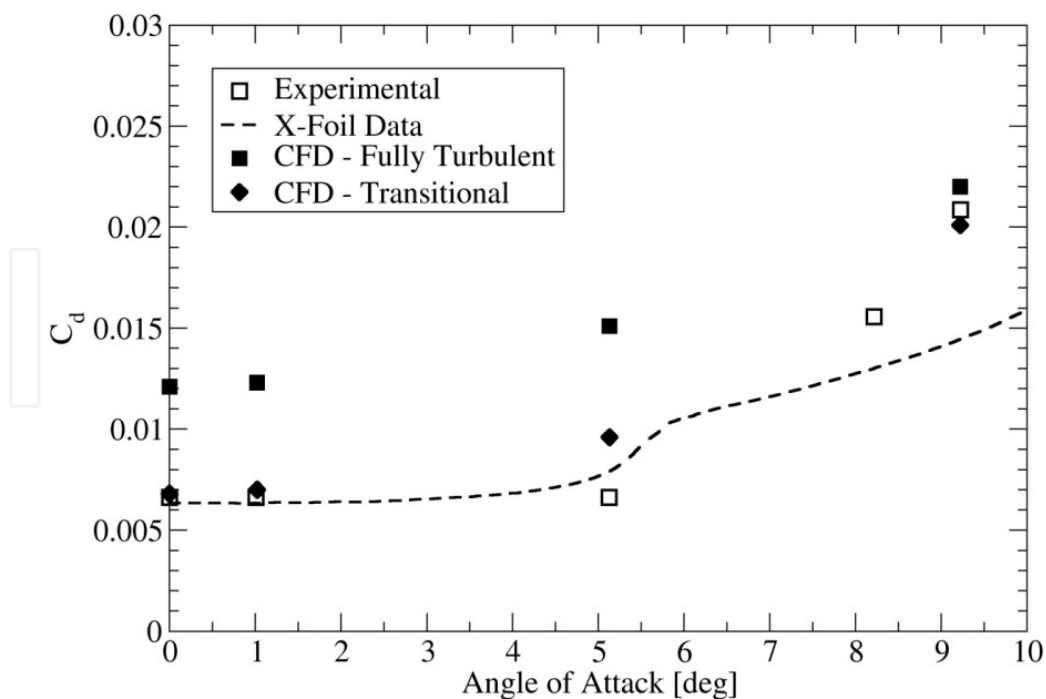
Fig. 14. Lift Coefficient (Cl) Polar for the S809 airfoil.

Fig. 15. Drag Coefficient (Cd) Polar for the S809 airfoil The results obtained for the lift and drag polars are.

4. Conclusions

In this chapter various methods for transition prediction in general purpose CFD codes have been discussed. In addition, the requirements that a model has to satisfy to be suitable for implementation into a general purpose CFD code have been listed. The main criterion is that non-local operations must be avoided. A new concept of transition modeling termed Local Correlation-based Transition Model (LCTM) was introduced. It combines the advantages of locally formulated transport equations with the physical information contained in empirical correlations. The γ-Re$_θ$ transition model is a representative of that modeling concept. The model is based on two new transport equations (in addition to the k and ω equations), one for intermittency and one for a transition onset criterion in terms of momentum thickness Reynolds number. The proposed transport equations do not attempt to model the physics of the transition process (unlike e.g. turbulence models), but form a framework for the implementation of transition correlations into general-purpose CFD methods.

An overview of the γ-Re$_θ$ model formulation has been given along with the publication of the full model including some previously undisclosed empirical correlations that control the predicted transition length. The main goal of the present chapter was to publish the full model and release it to the research community so that it can continue to be further validated and possibly extended. Included in this chapter are a number of test cases that can be used to validate the implementation of the model in a given CFD code.

The present transition model accounts for transition due to freestream turbulence intensity, pressure gradients and separation. It is fully CFD-compatible and does not negatively affect

the convergence of the solver. Current limitations of the model are that crossflow instability or roughness are not included in the correlations and that the transition correlations are formulated non-Galilean invariant. These limitations are currently being investigated and can be removed in principle

An overview of the test cases computed with the new model has been given. Due to the nature of the chapter, the presentation of each individual test case had to be brief. More details on the test case set-up, boundary conditions grid resolutions etc. can be found in the references. The purpose of the overview was to show that the model can handle a wide variety of geometries and physically diverse problems.

The authors believe that the current model is a significant step forward in engineering transition modeling. Through the use of transport equations instead of search or line integration algorithms, the model formulation offers a flexible environment for engineering transition predictions that is fully compatible with the infrastructure of modern CFD methods. As a result, the model can be used in any general purpose CFD method without special provisions for geometry and grid topology. The authors believe that the LCTM concept of combining transition correlations with locally formulated transport equations has a strong potential for allowing the 1st order effects of transition to be included into today's industrial CFD simulations.

5. Acknowledgments

6. References

[1] Schlichting, H., 1979, Boundary Layer Theory, McGraw-Hill, 7th edition.
[2] Morkovin, M.V., 1969, "On the Many Faces of Transition", Viscous Drag Reduction, C.S. Wells, ed., Plenum Press, New York, pp 1-31.
[3] Malkiel, E. and Mayle, R.E., 1996, "Transition in a Separation Bubble," ASME Journal of Turbo machinery, Vol. 118, pp. 752-759.
[4] Mayle, R.E., 1991, "The Role of Laminar-Turbulent Transition in Gas Turbine Engines," Journal of Turbomachinery, Vol. 113, pp. 509-537.
[5] Smith, A.M.O. and Gamberoni, N., 1956, "Transition, Pressure Gradient and Stability Theory," Douglas Aircraft Company, Long Beach, Calif. Rep. ES 26388.
[6] Van Ingen, J.L., 1956, "A suggested Semi-Empirical Method for the Calculation of the Boundary Layer Transition Region," Univ. of Delft, Dept. Aerospace Engineering, Delft, The Netherlands, Rep. VTH-74.

[7] Stock, H.W. and Haase, W., 2000, "Navier-Stokes Airfoil Computations with e^N Transition Prediction Including Transitional Flow Regions," AIAA Journal, Vol. 38, No. 11, pp. 2059 – 2066.

[8] Drela, M., and Giles, M. B., 1987, "Viscous-Inviscid Analysis of Transonic and Low Reynolds Number Airfoils", AIAA Journal, Vol. 25, pp. 1347 – 1355.

[9] Youngren, H., and Drela, M., 1991, "Viscous-Inviscid Method for Preliminary Design of Transonic Cascades", AIAA Paper No. 91-2364.

[10] Jones, W. P., and Launder, B. E., 1973, "The Calculation of Low Reynolds Number Phenomena with a Two-Equation Model of Turbulence", Int. J. Heat Mass Transfer, Vol. 15, pp. 301-314.

[11] Rodi, W. and Scheuerer, G., 1984, "Calculation of Laminar-Turbulent Boundary Layer Transition on Turbine Blades", AGARD CP 390 on Heat transfer and colloing in gas turbines.

[12] Savill, A.M., 1993, Some recent progress in the turbulence modeling of by-pass transition, In: R.M.C. So, C.G. Speziale and B.E. Launder, Eds.: Near-Wall Turbulent Flows, Elsevier, p. 829.

[13] Savill, A.M., 1996, One-point closures applied to transition, Turbulence and Transition Modeling, M. Hallbäck et al., eds., Kluwer, pp. 233-268.

[14] Wilcox, D.C.W. (1994). Simulation of transition with a two-equation turbulence model, *AIAA J.* Vol. 32, No. 2.

[15] Langtry, R.B., and Sjolander, S.A., 2002, "Prediction of Transition for Attached and Separated Shear Layers in Turbomachinery", AIAA Paper 2002-3643.

[16] Walters, D.K and Leylek, J.H., 2002, "A New Model for Boundary-Layer Transition Using a Single-Point RANS Approach", ASME IMECE'02, IMECE2002-HT-32740.

[17] Abu-Ghannam, B.J. and Shaw, R., 1980, "Natural Transition of Boundary Layers -The Effects of Turbulence, Pressure Gradient, and Flow History," Journal of Mechanical Engineering Science, Vol. 22, No. 5, pp. 213 – 228.

[18] Mayle, R.E., 1991, "The Role of Laminar-Turbulent Transition in Gas Turbine Engines," Journal of Turbomachinery, Vol. 113, pp. 509-537.

[19] Suzen, Y.B., Huang, P.G., Hultgren, L.S., Ashpis, D.E., 2003, "Predictions of Separated and Transitional Boundary Layers Under Low-Pressure Turbine Airfoil Conditions Using an Intermittency Transport Equation," Journal of Turbomachinery, Vol. 125, No. 3, July 2003, pp. 455-464.

[20] Durbin, P.A., Jacobs, R.G. and Wu, X., 2002, "DNS of Bypass Transition," Closure Strategies for Turbulent and Transitional Flows, edited by B.E. Launder and N.D. Sandham, Cambridge University Press, pp. 449-463.

[21] Van Driest, E.R. and Blumer, C.B., 1963, "Boundary Layer Transition: Freestream Turbulence and Pressure Gradient Effects," AIAA Journal, Vol. 1, No. 6, June 1963, pp. 1303-1306.

[22] Menter, F.R., Esch, T. and Kubacki, S., 2002, "Transition Modelling Based on Local Variables", 5th International Symposium on Engineering Turbulence Modelling and Measurements, Mallorca, Spain.

[23] Walters K. Cokljat, D., (2008), "A Three-Equation Eddy-Viscosity Model for Reynolds-Averaged Navier–Stokes Simulations of Transitional Flow", J. Fluids Eng., Volume 130, Issue 12.

[24] Pacciani R., Marconcini M., Fadai-Ghotbi A., Lardeau S., Leschziner, M. A., 2009, "Calculation of High-Lift Cascades in Low Pressure Turbine Conditions Using a Three-Equation Model" ASME Turbo Expo, Orlando, FL, USA, 8-12 June, ASME paper GT2009-59557. Conf. Proc. Vol. 7: Turbomachinery, Parts A and B, pp. 433-442. ISBN 978-0-7918-4888-3.

[25] Langtry, R.B., Menter, F.R., 2009, "Correlation-Based Transition Modeling for Unstructured Parallelized Computational Fluid Dynamics Codes", AIAA J. Vol. 47, No.12,

[26] Cutrone L., De Palma P., Pascazio G., and Napolitano M., 2008, "Predicting transition in two- and three-dimensional separated flows", Int. J. Heat Fluid Fl 29 504–526.

[27] S. Fu and L. Wang, 2008,: "Modelling the flow transition in supersonic boundary layer with a new k–ω−γ transition/turbulence model", in: 7th International Symposium on Engineering Turbulence Modelling and Measurements-ETMM7, Limassol, Cyprus.

[28] Serdar Genec, M., Kaynak and Ü. Yapıcı, H., 2011,: "Performance of Transition Model for Predicting Low Re Aerofoil Flows without/with Single and Simultaneous Blowing and Suction" European Journal of Mechanics B/Fluids, vol 30 (2), pp. 218-235, 2011.

[29] Menter, F.R., Langtry, R.B., Likki, S.R., Suzen, Y.B., Huang, P.G., and Völker, S., 2006, "A Correlation based Transition Model using Local Variables Part 1- Model Formulation", ASME Journal of Turbomachinery, Vol. 128, Issue 3, pp. 413 – 422.

[30] Langtry, R.B., Menter, F.R., Likki, S.R., Suzen, Y.B., Huang, P.G., and Völker, S., 2006, "A Correlation based Transition Model using Local Variables Part 2 - Test Cases and Industrial Applications", ASME Journal of Turbomachinery, Vol. 128, Issue 3, pp. 423 – 434.

[31] Menter, F.R., Langtry, R.B. and Völker, S., 2006, "Transition Modelling for General Purpose CFD Codes", Journal of Flow, Turbulence and Combustion, Vol. 77, Numbers 1 – 4, pp. 277-303.

[32] Menter, F.R., 1994, "Two-Equation eddy-viscosity turbulence models for engineering applications", AIAA Journal, Vol. 32, No. 8, pp. 1598-1605.

[33] Langtry, R.B., 2006, "A Correlation-Based Transition Model using Local Variables for Unstructured Parallelized CFD codes", Doctoral Thesis, University of Stuttgart. http://elib.uni-stuttgart.de/opus/volltexte/2006/2801/

[34] Fashifar, A. and Johnson, M. W., 1992, "An Improved Boundary Layer Transition Correlation", ASME Paper ASME-92-GT-245.

[35] Schubauer, G.B. and Skramstad, H.K., 1948, "Laminar-boundary-layer oscillations and transition on a flat plate," NACA Rept. 909.

[36] Sinclair, C. and Wells, Jr., 1967, "Effects of Freestream Turbulence on Boundary-Layer Transition," AIAA Journal, Vol. 5, No. 1, pp. 172-174.

[37] Schubauer, G.B. and Klebanoff, P.S., (1955), "Contribution on the Mechanics of Boundary Layer Transition," NACA TN 3489.

[38] McIlroy, H.M. and Budwig, R.S., (2005). "The Boundary Layer over Turbine Blade Models with Realistic Rough Surfaces", *ASME-GT2005-68342, ASME TURBO EXPO 2005*, Reno-Tahoe, Nevada, USA.

[39] Zierke, W.C. and Deutsch, S., 1989, "The measurement of boundary layers on a compressor blade in cascade – Vols. 1 and 2", NASA CR 185118.

[40] Dorney, D.J., Lake, J.P., King, P.L. and Ashpis, D.E., 2000, "Experimental and Numerical Investigation of Losses in Low-Pressure Turbine Blade Rows," AIAA Paper AIAA-2000-0737, Reno, NV.

[41] Huang, J., Corke, T.C., Thomas, F.O., 2003, "Plasma Actuators for Separation Control of Low Pressure Turbine Blades", AIAA Paper No. AIAA-2003-1027.

[42] Arts, T., Lambert de Rouvroit, M., Rutherford, A.W., 1990, "Aero-Thermal Investigation of a Highly Loaded Transonic Linear Turbine Guide Vane Cascade", von Karman Institute for Fluid Dynamics, Technical Note 174.

[43] Steelant, J., and Dick, E., 2001, "Modeling of Laminar-Turbulent Transition for High Freestream Turbulence", Journal of Fluids Engineering, Vol. 123, pp. 22-30.

[44] Somers, D.M., "Design and Experimental Results for the S809 Airfoil", Airfoils, Inc., State College, PA, 1989.

[45] Somers, D.M., "Design and Experimental Results for the S809 Airfoil", NREL/SR-440-6918, January 1997.

[46] Langtry, R.B., Gola, J. and Menter, F.R. 2006, "Predicting 2D Airfoil and 3D Wind Turbine Rotor   Performance using a Transition Model for General CFD Codes", AIAA Paper 2006-0395.
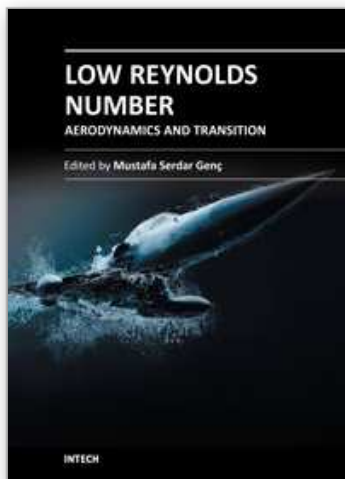
Low Reynolds Number Aerodynamics and Transition

Edited by Dr. Mustafa Serdar Genc

This book reports the latest development and trends in the low Re number aerodynamics, transition from laminar to turbulence, unsteady low Reynolds number flows, experimental studies, numerical transition modelling, control of low Re number flows, and MAV wing aerodynamics. The contributors to each chapter are fluid mechanics and aerodynamics scientists and engineers with strong expertise in their respective fields. As a whole, the studies presented here reveal important new directions toward the realization of applications of MAV and wind turbine blades.

How to reference

In order to correctly reference this scholarly work, feel free to copy and paste the following:

F. R. Menter and R. B. Langtry (2012). Transition Modelling for Turbomachinery Flows, Low Reynolds Number Aerodynamics and Transition, Dr. Mustafa Serdar Genc (Ed.), ISBN: 978-953-51-0492-6, InTech, Available from: http://www.intechopen.com/books/low-reynolds-number-aerodynamics-and-transition/transition-modelling-for-turbomachinery-flows

INTECH
open science | open minds